Article

Chemistry & Biology

Membrane Protein 4F2/CD98 Is a Cell Surface Receptor Involved in the Internalization and Trafficking of Human β-Defensin 3 in Epithelial Cells

Graphical Abstract

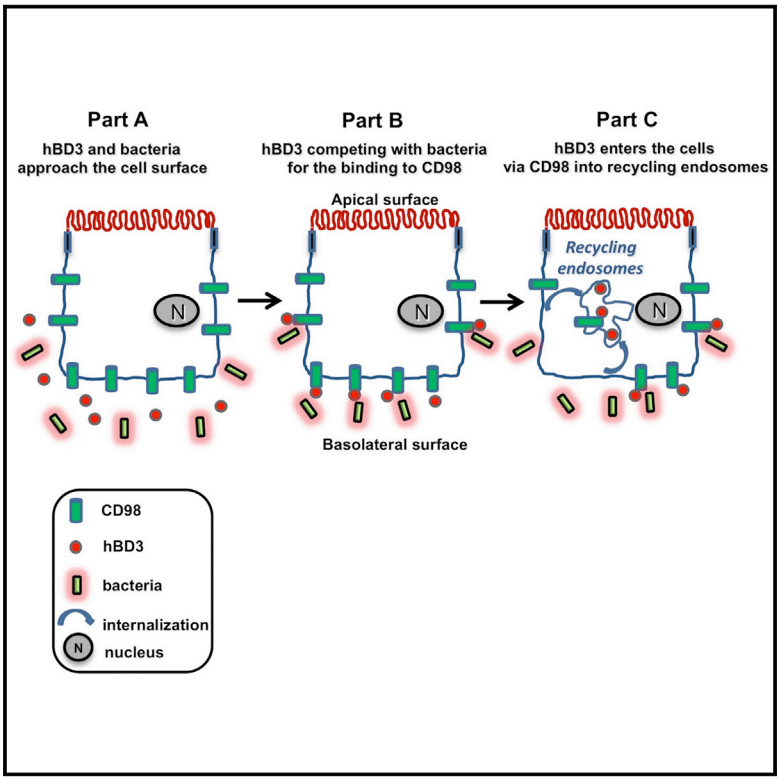

Authors

Irene Colavita, Ersilia Nigro, ..., Antonello Pessi, Francesco Salvatore

Correspondence

salvator@unina.it (F.S.), a.pessi@peptipharma.it (A.P.)

In Brief

Colavita et al. show that CD98 is a receptor that mediates hBD3 internalization in epithelial cells. The region involved in hBD3 binding overlaps with the area known to interact with intestinal bacteria. This suggests a novel mechanism of antibacterial action for defensins.

Highlights

- Proteomics of hBD3 at the cell surface indicates that CD98 is a receptor
- hBD3 reduces CD98 expression in epithelial cells
- Trafficking into epithelial cells occurs through recycling endosomes
- hBD3 binding to CD98 with high affinity may represent a novel antibacterial mechanism

Colavita et al., 2015, Chemistry & Biology 22, 217–228
February 19, 2015
http://dx.doi.org/10.1016/j.chembiol.2014.11.020

Chemistry & Biology
Article

Membrane Protein 4F2/CD98 Is a Cell Surface Receptor Involved in the Internalization and Trafficking of Human β-Defensin 3 in Epithelial Cells

Irene Colavita,[1,6] Ersilia Nigro,[1,6] Daniela Sarnataro,[1,2] Olga Scudiero,[1,2] Vincenzo Granata,[1] Aurora Daniele,[1,3] Adriana Zagari,[1] Antonello Pessi,[1,4,*] and Francesco Salvatore[1,5,*]
[1]CEINGE-Biotecnologie Avanzate S.c.a r.l., Via Gaetano Salvatore 486, 80145 Naples, Italy
[2]Dipartimento di Medicina Molecolare e Biotecnologie Mediche, Università degli Studi di Napoli Federico II, Via Sergio Pansini 5, 80131 Naples, Italy
[3]Dipartimento di Scienze e Tecnologie Ambientali Biologiche Farmaceutiche, Seconda Università degli Studi di Napoli, Via Vivaldi 43, 81100 Caserta, Italy
[4]PeptiPharma, Viale Città D'Europa 679, 00144 Rome, Italy
[5]IRCCS-Fondazione SDN, Via Emanuele Gianturco 113, 80142 Naples, Italy
[6]Co-first author
*Correspondence: salvator@unina.it (F.S.), a.pessi@peptipharma.it (A.P.)
http://dx.doi.org/10.1016/j.chembiol.2014.11.020

SUMMARY

Human β-defensins play a pivotal role in the innate immune response. Although expressed by and acting at epithelial surfaces, little is known about their specific interaction with epithelial structures. Here, we identify the transmembrane protein CD98 as a cell surface receptor involved in the internalization of human β-defensin 3 (hBD3) in human epithelial A549 cells. CD98 and hBD3 extensively colocalize on the basolateral domain of A549. While verifying their direct binding by fluorescence resonance energy transfer and surface plasmon resonance, we mapped the interaction to CD98 residues 304–414, i.e. to the region known to interact with the proteins of intestinal bacteria during colonic invasion. Treatment of A549 cells with hBD3 dramatically reduces CD98 expression and conversely, knockdown of CD98 expression impairs hBD3 cell surface binding and internalization. Competition for bacterial binding to CD98 and downregulation of CD98 expression may represent novel mechanisms for the antibacterial activity of hBD3.

INTRODUCTION

Human β-defensins (hBDs) are cationic peptides that play a pivotal role in the innate immune response. They display strong chemotactic activity toward immune cells, activating and amplifying the adaptive immune response. Moreover, hBDs exert antimicrobial activity against a wide spectrum of bacteria and viruses, through binding to the plasma membrane of pathogens and subsequent pore formation (Dhople et al., 2006; Semple and Dorin, 2012; Yamaguchi and Ouchi, 2012; Sudheendra et al., 2014). To date, more than 6 hBDs have been identified but the best characterized are hBD1–4 (Jarczak et al., 2013). Their antimicrobial activities have been extensively studied and much effort was made to design more potent analogs. Another aspect that has been investigated is maintenance of antimicrobial activity in the presence of high salt concentration, such as observed in the respiratory epithelia of patients with cystic fibrosis (Smith et al., 1996). While hBD1, 2, and 4 are inactivated by high salt conditions, hBD3 is salt resistant, and hence more attractive for therapeutic use (Ganz, 2003; Sass et al., 2010; Harder et al., 2001). The combination of high potency and salt resistance was also investigated previously by us with hDB1/hBD3 chimeras to enhance the potency and breadth of their antibacterial activity (Scudiero et al., 2010, 2013).

All hBDs contain six highly conserved cysteine (Cys) residues, which dictate a rigid conformation stabilized by three disulfide bridges. Most hBDs are amphipathic, with a net positive charge that confers on them features similar to cell-penetrating peptides, short positively charged amphipathic peptides that penetrate biological membranes (Zorko and Langel, 2005). In particular, hBD3 is the protein product of the human gene *DEFB103* and belongs to the naturally occurring supercharged human proteins (NSHPs), which can penetrate human cells (Cronican et al., 2011; Thompson et al., 2012) and, with a net charge of +11, has the highest charge to mass ratio in NSHPs. All hBDs are secreted by epithelia, and their expression is upregulated in the course of infection and inflammation in order to act as a chemical barrier against pathogens (Semple and Dorin, 2012). However, although epithelia represent the natural site of action of these peptides, little is known about the interaction of hBDs with human epithelial cells.

We previously showed that hBD1, hBD3, and hBD1/hBD3 chimeras are not toxic to human epithelial cell lines and that they are internalized into the cytoplasm via an active endocytic mechanism (Scudiero et al., 2010). Consistent with our findings, hBD3 fused to the mCherry fluorophore was also shown to be able to penetrate human cells (Cronican et al., 2011). We have now analyzed in greater detail the interaction of hBD3 with the human pulmonary epithelial cell line A549. In particular, we addressed the question of whether hBD3 internalization is mediated by specific receptors on epithelial cells, as described for the receptors

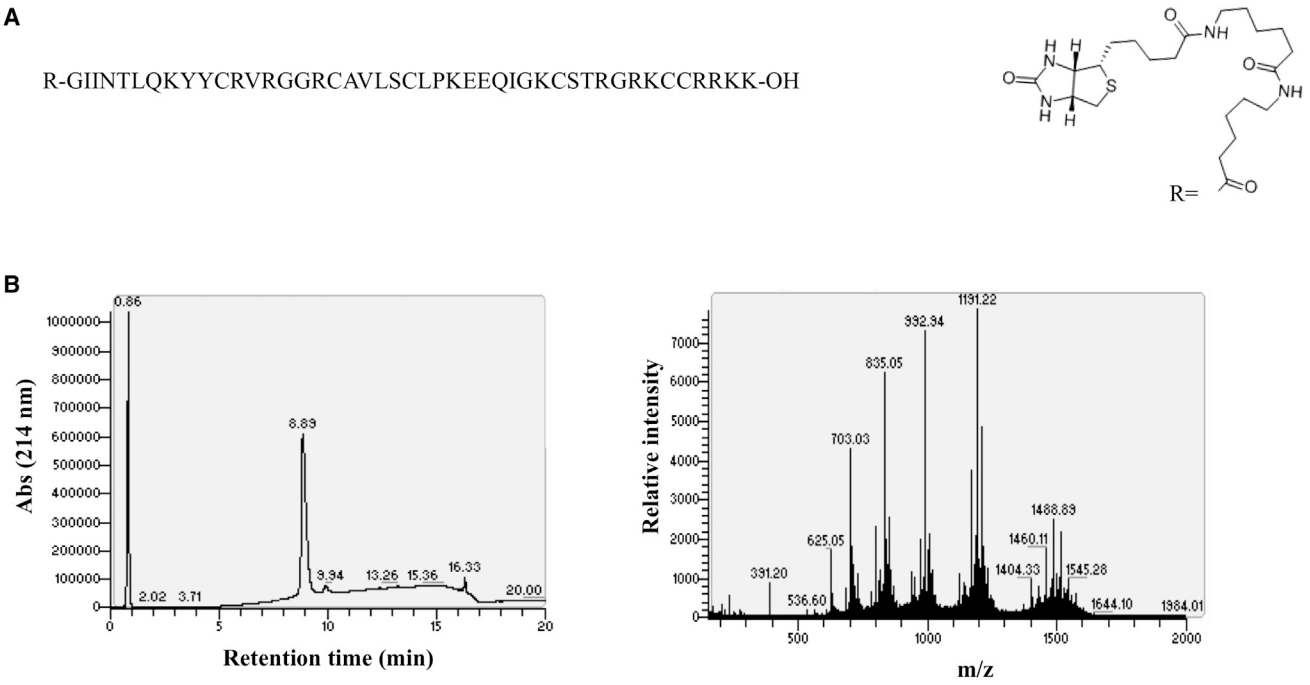

Figure 1. Synthesis of Biotin-2X-hBD3

(A) Structure of the Biotin-2X-hBD3 peptide (Biotin-2X has a side chain to the cyclic part of the molecule of two more 5-carbon chains that bind to the N-terminal glycine of hBD3) used to identify hBD3 membrane protein interactors. hBD3 has a net positive charge of +11.

(B) Biotin-2X-hBD3 was identified by positive ESI LC-MS. Analytical RP-HPLC (left panel) was performed with a reverse-phase C18 column using as solvent system H_2O/0.1 TFA and CH_3CN/0.1% TFA, and a linear gradient 5%–50% of CH_3CN/0.1% TFA over 17 min, at a flow rate of 1 ml/min. The ESI + full MS spectrum (right panel, mass range: 150–2,000 Da) shows the Biotin-2X-hBD3 multicharged ions in the range of 8.76–9.33 min, which corresponds to the peptide retention time. The theoretical mass of the peptide is 5614 Da. See also Figure S1.

expressed on immune cells, the binding of which also triggers chemotaxis (Soruri et al., 2007; Röhrl et al., 2010). In this context, it is noteworthy that hBD3 has been implicated in the modulation of melanocortin receptors (Beaumont et al., 2012; Nix et al., 2013). Our analysis identifies 4F2/CD98 as an hBD3-specific membrane receptor and shows that it is internalized by means of recycling endosomes.

RESULTS

Internalization and Trafficking of Biotin-Labeled hBD3

Synthesis of Biotin-Labeled hBD3

We used biotin as label. Biotin was incorporated at the N terminus of the peptide using standard solid-phase peptide synthesis (Figure 1). Unless otherwise specified, we used the fully reduced, purified peptide, since the antibacterial activity of hBD3 does not differ between the oxidized (hereafter referred to as hBD3ox) and reduced forms (Scudiero et al., 2013), as also shown in Figure S1.

Biotin-Labeled hBD3 Maintains Antibacterial Activity against Escherichia coli

To ensure that biotin did not alter the antibacterial properties of hBD3, we tested Biotin-2X-hBD3 against *Escherichia coli* in comparison with reduced and oxidized unlabeled hBD3 using two concentrations of peptide (2.5 and 12.5 μM), and four concentrations of NaCl (0.0, 50, 100, and 200 mM) (Figure S1). The minimum inhibitory concentration ranged between 12.5 and 25.0 μM for all the peptides, thereby confirming that biotinylation does not impair the antibacterial activity of hBD3.

hBD3 Localizes at the Basolateral Plasma Membrane of Polarized Epithelial A549 Cells from which It Is Internalized through Recycling Endosomes

To explore the localization of hBD3 on the plasma membrane, we incubated Biotin-2X-hBD3 with live epithelial cells cultured on a transwell filter, both apically and basolaterally, for 20 min at 4°C (pulse), then with streptavidin-Cy3 conjugated, and lastly with E-cadherin, a marker of the basolateral plasma membrane (Miranda et al., 2003). As shown in Figure 2A, Biotin-2X-hBD3 extensively colocalized with E-cadherin at the basolateral domain of the A549 plasma membrane.

We (Scudiero et al., 2013) and others (Mburu et al., 2011) previously reported that hBD3 is able to enter mammalian cells via an active endocytic mechanism. To investigate the mechanism of hBD3 entry, we specifically labeled recycling endosomes using a transferrin-Alexa488 conjugate. A549 cells were incubated with the peptide and transferrin-Alexa488 for 20 min at 4°C (pulse) and then at 37°C for different chase times. Biotin-2X-hBD3 extensively colocalizes with transferrin up to 30 min of chase after 0 min, 15 min, and 30 min of chase (Figure 2B), indicating that internalization is largely driven through recycling endosomes. Internalization via early endosomes and localization to the lysosomal pathway was ruled out by lack of colocalization of hBD3 with either the early endosome marker EE1 or with the endo/lysosomal marker LAMP-1 after 0 min, 15 min, and

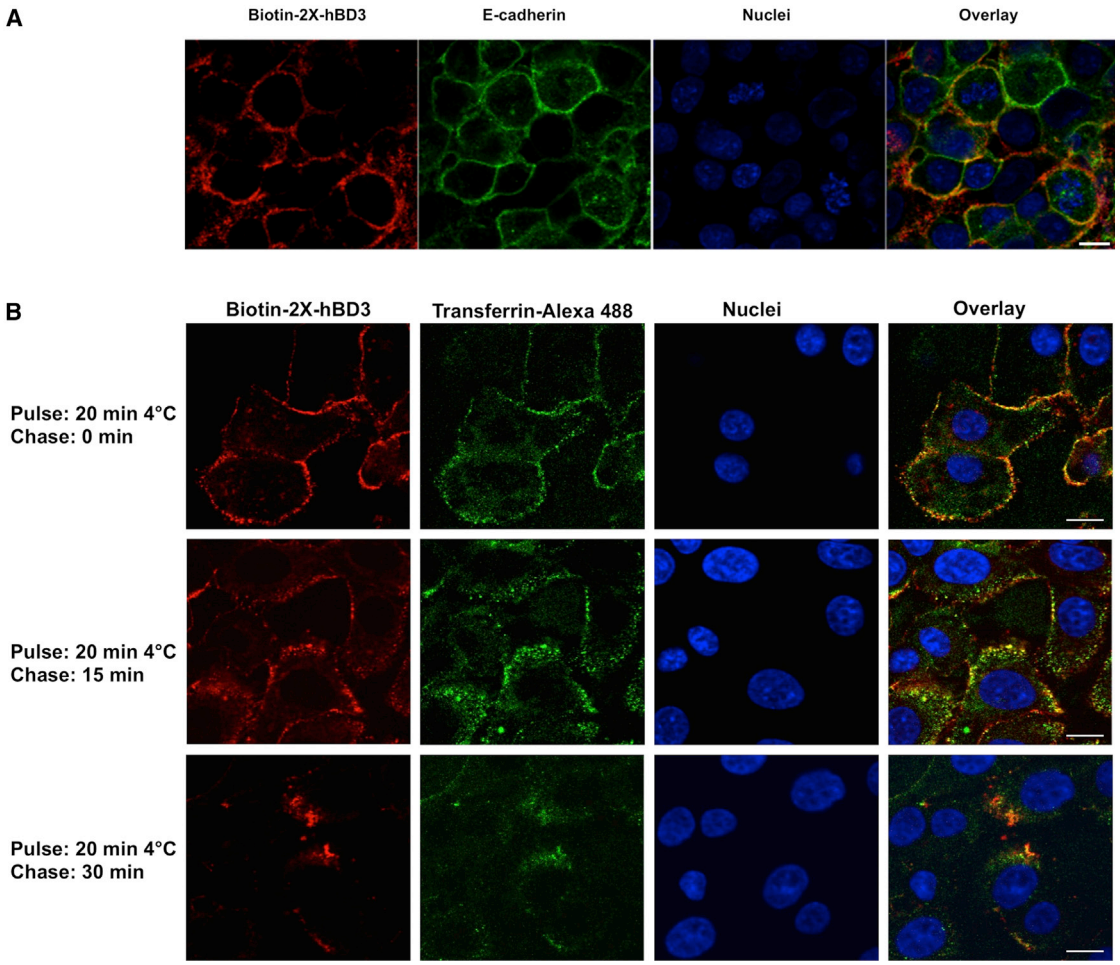

Figure 2. Biotin-2X-hBD3 Specifically Distributes on the Basolateral Domain of the Plasma Membrane

(A) A549 cells, grown on a filter for 72 hr, were incubated with the peptide (10 μM) for 20 min at 4°C (pulse), washed and labeled with streptavidin-Cy3 and a marker of the basolateral cell membrane (E-cadherin). Scale bars, 10 μm. Images represent single 1-μm-thick optical slices. Biotin-2X-hBD3 is red, E-cadherin green, and nuclei blue; colocalization appears orange-yellow in the overlay image. Results are from three independent experiments, with ≥100 cells per experiment. (B) Biotin-2X-hBD3 colocalizes with transferrin into recycling endosomes. A549 cells were incubated with the peptide (10 μM) and with a marker of recycling endosomes (transferrin-Alexa488 conjugated) for 20 min at 4°C (pulse), washed and incubated at 37°C for different chase times. Scale bars, 10 μm. Images represent single 1-μm-thick optical slices. Biotin-hBD3 is red, transferrin-Alexa488 is green, nuclei are blue; colocalizing regions appear orange-yellow in the overlay image. Three independent experiments were performed, and images were acquired from at least 100 cells per experiment.

30 min of chase throughout the kinetics of the endocytic assays (data not shown).

Functional Proteomics Identifies 4F2/CD98 as a Putative Interactor of hBD3

To identify hBD3 interactors on the plasma membrane of A549 cells, we applied a functional proteomic approach using Biotin-2X-hBD3 as a bait to capture interacting membrane proteins (Figure S2). Biotin-2X-hBD3 was incubated with A549 cells as reported in Experimental Procedures. Cells were then subjected to subcellular fractionation to isolate membrane components. The efficiency of subcellular fractionation was evaluated by Western blotting (see Figure S3A). The Biotin-2X-hBD3 crosslinked complexes were purified by affinity chromatography using streptavidin magnetic beads (see also Figure S2). Protein extract from cells incubated with Biotin-2X alone was used as negative control. Then, the protein partners were eluted and decrosslinked, as described elsewhere (Sutherland et al., 2008; Klockenbusch and Kast, 2010) (see Figure S3B), fractionated by SDS-PAGE, stained, and submitted to mass spectrometry for protein identification.

Among the 19 proteins identified in this study, we focused on 4F2/CD98, which is a membrane protein involved in *L*-type amino acid transport, in integrin-mediated cell adhesion, and notably, in inflammation and in the immune response (Nguyen et al., 2011; Nguyen and Merlin, 2012). We observed the CD98 protein in cells treated with Biotin-2X-hBD3 but not in those treated with Biotin-2X alone (Figure 3A, lanes 1 and 2). Western blot analysis of the proteins obtained from Biotin-2X-hBD3 crosslinking yielded positive staining with an anti-CD98 antibody, whereas no significant staining was observed for the control samples from the control biotin crosslinking (Figure 3B).

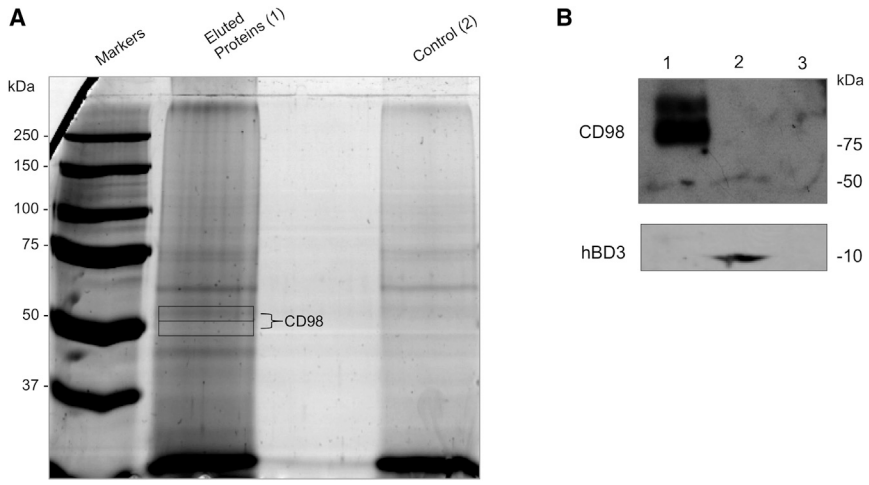

Figure 3. Functional Proteomics Identifies 4F2/CD98 as a Putative Interactor of hBD3

(A) Separation of Biotin-2X-hBD3-interacting membrane proteins (lane 1) in A549 cells. The gel was stained with Coomassie brilliant blue and bands were excised and subjected to LC-MS/MS analysis. Peptide-protein complexes from cells incubated with Biotin-2X only and eluted from streptavidin beads was used as control (lane 2). The CD98 protein, identified by LC-MS/MS analysis, is boxed. Lane 1 shows the molecular weight markers. (B) Western blot analysis of Biotin-2X-hBD3 complexes isolated by affinity purification with anti-CD98 and anti-hBD3. Lane 1: membrane proteins crosslinked to the Biotin-2X-hBD3 peptide, used as input for the affinity chromatography experiment. Lane 2: Biotin-2X-hBD3 complexes eluted from streptavidin beads and decrosslinked. Lane 3: peptide-protein complexes from cells incubated with Biotin-2X without hBD3, and eluted from streptavidin beads used as control. See also Figures S2 and S3.

Confocal Microscopy Confirms the hBD3-CD98 Interaction on the Cell Surface

Cell surface interaction of CD98 with Biotin-2X-hBD3 was confirmed by confocal microscopy (Figure 4A). A549 cells incubated with the peptide for 20 min at 4°C and then immunostained with CD98, Biotin-2X-hBD3, and CD98 extensively colocalized at the basolateral membrane (Figure 4A). Confocal microscopy of cells fixed and coimmunostained with CD98 and Biotin-2X-hBD3 showed about 11% of fluorescence resonance energy transfer (FRET) efficiency measured by the acceptor photobleaching technique (Figure 4B), a value indicating that the two partners are close enough to allow energy transfer. Indeed, acceptor bleaching (Biotin-2X-hBD3 labeled with streptavidin Cy5) resulted in a significant increase of donor (CD98 Cy3) emission in cells labeled with hBD3 and CD98. We found FRET when we bleached selected plasma membrane regions of interest. The percentage of FRET efficiency is shown in Figure 4C.

To verify the specificity of hBD3 binding to CD98, we performed a competition binding assay (see Figure 5). First, we used a titration curve to determine the optimal peptide concentration that resulted in a linear correspondence between concentration and fluorescence signal (Figure 5A), and selected 3 μM Biotin-2X-hBD3. Then, we performed the competition binding assay in two distinct setups: (1) preincubation of Biotin-2X-hBD3 for 20 min at 4°C followed by hBD3 for a further 20 min at 4°C (Figure 5B[b,c]); and (2) preincubation of hBD3 for 20 min at 4°C followed by Biotin-2X-hBD3 for a further 20 min at 4°C (Figure 5B[d,e]). In cells pretreated with unlabeled hBD3, there was a notable decrease of Biotin-2X-hBD3 binding; conversely, fluorescence was not affected when the incubation of cold hBD3 was performed after exposure to labeled Biotin-2X-hBD3. This suggests that once hBD3 binds to cells, the subsequent incubation with Biotin-2X-hBD3 is not able to displace the binding of the peptide from the plasma membrane. These data indicate that hBD3 binding to the cell membrane is specific and occurs with a good affinity, which is consistent with the value of the dissociation constant (KD) (see Table 1).

Trafficking of hBD3 and CD98 after Internalization

We then monitored the fate of CD98 after binding to hBD3 (Figure 6A). A549 cells were incubated with the peptide for 20 min at 4°C, then at 37°C for different chase times, and immunostained with CD98. Starting from the plasma membrane, where the two partners colocalize, we found that Biotin-2X-hBD3 colocalized with CD98 in endocytic vesicles at different chase times (Figure 6A), which is in agreement with the observation that hBD3 is internalized by means of recycling endosomes and accumulates with transferrin (Figure 2B).

Silencing of CD98 Prevents Binding and Internalization of hBD3

We tested the effect of silencing on the synthesis of CD98 by specific small interfering RNA (siRNA) interference. The higher efficiency of the CD98-specific siRNA molecule versus a nonspecific scrambled control was confirmed by Western blot (Figure S4A) and by confocal microscopy (Figure S4B). A comparison of the Biotin-2X-hBD3 signal in CD98-knockdown A549 cells versus nontreated cells (Figure 6B) revealed that, in the silenced cells, hBD3 was neither able to bind the plasma membrane nor to enter the cells. Therefore, consistent with the images shown in Figure 4A, these results support the concept that hBD3 binding on the cell membrane is effectively dependent on CD98 expression.

Treatment of A549 Cells with hBD3 Leads to Reduced CD98 Expression

In a complementary experiment, we observed that treatment of A549 cells with Biotin-2X-hBD3 resulted in a decrease in the amount of CD98 24 hr post treatment (Figure S5). This is similar to the HIV coreceptor CXCR4, the internalization and downregulation of which are modulated by both hBD2 and hBD3 (Quiñones-Mateu et al., 2003; Feng et al., 2006).

Characterization of the CD98-hBD3 Interaction by Surface Plasmon Resonance

The molecular interaction between CD98 and hBD3 was further studied by surface plasmon resonance (SPR) (see also Figures S6A and S6B) (Jason-Moller et al., 2006). To identify the

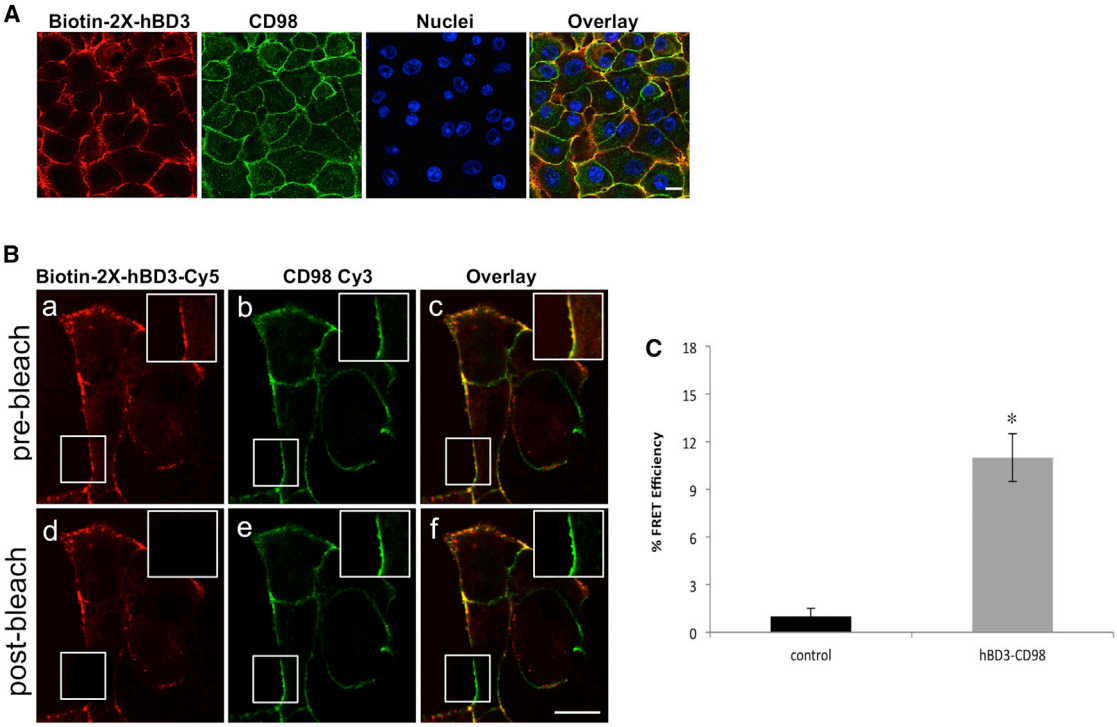

Figure 4. Biotin-2X-hBD3 Colocalizes and Directly Interacts with CD98

(A) A549 cells were grown on filters for 72 hr, incubated with the peptide (10 μM) for 20 min at 4°C (pulse), then washed and immunostained with CD98. Biotin-2X-hBD3 colocalized with CD98 at 0 min. Scale bars, 10 μm. Images represent single 1-μm-thick optical slices. Biotin-2X-hBD3 is red, CD-98 is green, nuclei labeled with DAPI are in blue; colocalization appears orange-yellow in the overlay image. Three independent experiments were performed, and images were acquired from ≥100 cells per experiment.

(B) hBD3/CD98 direct interaction. FRET was measured with the acceptor photobleaching technique as described in Experimental Procedures. The image shows the signal of biotinylated hBD3 (red) and CD98 (green) before (a, b, c prebleach) and after (d, e, f postbleach) photobleaching. The selected regions of interest for bleaching are indicated.

(C) Energy transfer efficiency was measured in cells immunostained for Biotin-2X-hBD3 and CD98 and is expressed in % as the mean of three independent experiments. Error bars: ± SD. *Highly significant difference ($p < 0.001$). See also Figures S4 and S5.

interacting regions of CD98, the three protein sequences shown in Figure 7A were selected, hereafter referred to as GST-CD98, GST-CD98cut, and CD98-6His. All proteins were covalently immobilized on the appropriate chip (see Experimental Procedures). Subsequently, both reduced and oxidized hBD3 solutions, at various concentrations, were allowed to flow on all the immobilized CD98 molecules. To verify the occurrence of binding, reduced hBD3 was covalently immobilized on a CM5 sensor chip. Then, a series of concentrations of all three CD98 sequences was allowed to flow on the immobilized hBD3.

Except for the GST-hBD3 pair, in which no interaction was detected, a ligand-analyte molecular interaction was detected in all measurements, in full agreement with the other data reported in this study. The SPR data were fitted using a two-state model to calculate the kinetic and equilibrium dissociation constants of the hBD3-CD98 complexes. KD values are reported in Table 1. These data confirm the occurrence of high-affinity binding between hBD3 and CD98 and in addition provide valuable insights into the interaction, as reported below.

First, the KD values are highly comparable for the two GST-fused CD98 sequences (2 and 3 in Figure 7A), going from the almost full-length M102-A630 protein to the short V304-H414 region, which unambiguously identifies the V304-H414 sequence as the interacting one. This region, which is part of the extracellular domain (see Figure 7A), is highly conserved; in fact, no variants have been described so far within this segment. Notably, the same region was shown by SPR to interact with proteins from enteropathogenic *E. coli* (EPEC) and *Citrobacter rodentium* (Shames et al., 2010; Charania et al., 2013).

Sequences 1 and 2 reported in Figure 7A, differing in tags and glycosylation, produce almost comparable SPR data, which differ by one order of magnitude in the strength of binding. Therefore, the abundant glycosylation in the human protein and the GST tag only slightly affect CD98 binding. Two of the four putative N-glycosylation sites, N365 and N381, are located in the interacting region on helical regions exposed to solvent, thereby leaving free access to the plasma membrane surface. Finally, the fully reduced and oxidized forms of hBD3 bind CD98 with comparable affinity, but with different kinetics. This behavior can be ascribed to the different 3D structure of the two forms.

DISCUSSION

While the extracellular activity of hBDs is reasonably well understood in terms of direct (e.g. pore formation in bacterial membranes) or indirect (e.g. chemotactic) antimicrobial activity, less

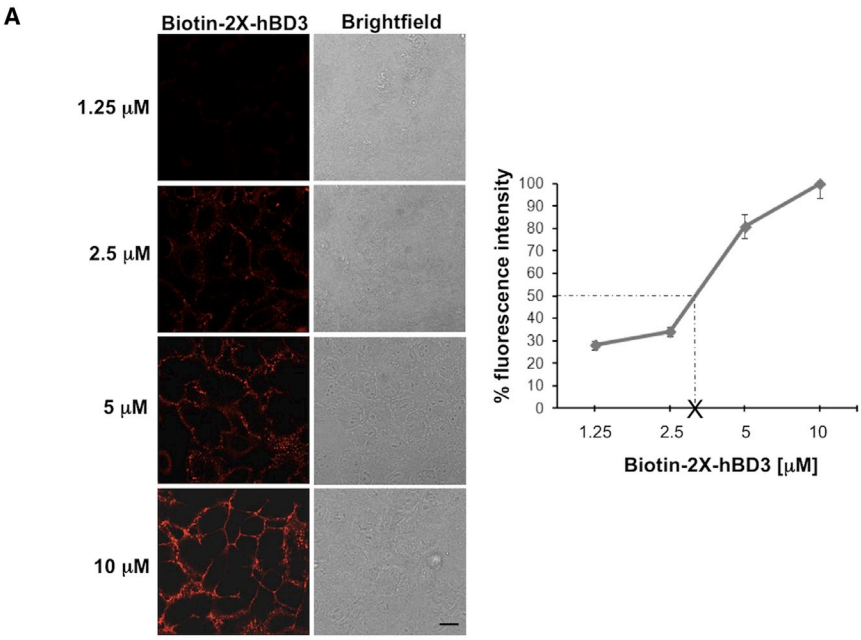

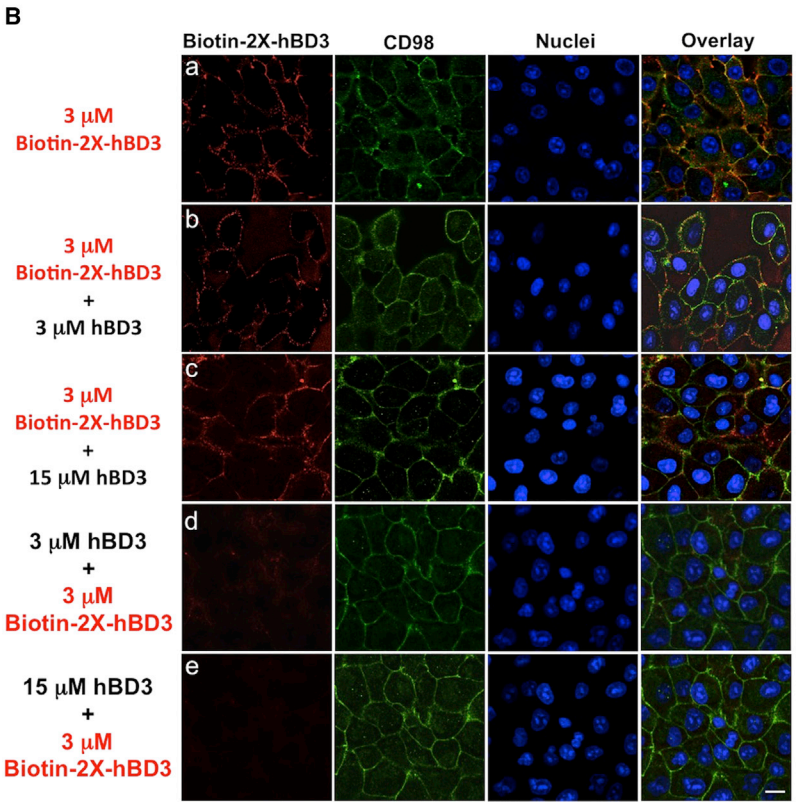

Figure 5. Competition Binding Assay of CD98 Versus Labeled and Unlabeled hBD3

(A) Titration curve. A549 cells were incubated with Biotin-2X-hBD3 (1.25, 2.5, 5, and 10 μM) for 20 min at 4°C. hBD3 was revealed by streptavidin-Cy3. Fluorescence intensity was measured by analyzing confocal images. Data represent means ± SD of three separate experiments in which each replicate reflects the fluorescence intensity from 25 cells/area.

(B) Competition assay. A549 cells were incubated with Biotin-2X-hBD3 (3 μM) for 20 min at 4°C (pulse), washed then incubated with hBD3 (3, 15 μM) and labeled with streptavidin-Cy3 (panels b, c). Conversely, the cells were incubated with unlabeled hBD3 (3, 15 μM) for 20 min at 4°C (pulse), washed then incubated with Biotin-2X-hBD3 (3 μM) and labeled with streptavidin-Cy3 (panels d, e). Scale bars, 10 μm. Images represent single 1-μm-thick optical slices.

is known about the intracellular role of these molecules. In the case of hBD3, we and others (Scudiero et al., 2013; Beaumont et al., 2012) previously reported that hBD3 is internalized in mammalian cells via an active endocytic mechanism. Moreover, a recent study devoted to the so-called NSHPs (Cronican et al., 2011), which are able to penetrate mammalian cells even more efficiently than the classic cell-penetrating peptides (Cronican et al., 2011; Thompson et al., 2012), showed that hBD3 has the highest charge/molecular mass ratio among NSHPs, and hBD3 fused to the mCherry fluorophore is able to penetrate HeLa, 3T3, and BSR cells (Cronican et al., 2011). However, little is known about hBD3 internalization in epithelial cells, which is the natural site of action of the molecule, and importantly, whether internalization is assisted by interaction with cell surface molecules.

Using a proteomic approach, we have identified a number of potential interactions between hBD3 and cell surface receptors in the human epithelial cell line A549. In particular, we have clarified the interaction of hBD3 with CD98, a type II transmembrane protein involved in *L*-type amino acid transport, in integrin-mediated cell adhesion, in inflammation (Kenworthy and Edidin, 1999), and in the immune response (Miranda et al., 2003). CD98 is involved in the innate host response to intestinal infection by enteric bacterial pathogens (Quiñones-Mateu et al., 2003). Its overexpression has been associated with increased expression of proinflammatory markers, with decreased expression of anti-inflammatory markers, and with increased attachment of EPEC and *C. rodentium* in mouse colon (Feng et al., 2006). The exposure of CD98 to the cellular lumen enables the enteropathogenic bacteria to directly access CD98, resulting in attachment and bacterially induced inflammation. In addition, CD98 is highly expressed in several tumors, including lung and breast, and its overexpression is associated with a poor

Table 1. Kinetic and Equilibrium Constants for the CD98-hBD3 Interaction based on SPR Data

CD98-hBD3 Interaction[a]	k_{on1} (×10^3/M/s)	k_{off1} (×10^{-2}/s)	k_{on2} (×10^{-3}/s)	k_{off2} (×10^{-3}/s)	KD (×10−7 M)
GST-CD98-hBD3[b]	4.27 ± 0.03	1.34 ± 0.02	5.73 ± 0.05	0.944 ± 0.004	4.43 ± 0.05
GST-CD98-hBD3[c]	8.51 ± 0.05	2.10 ± 0.03	9.03 ± 0.06	1.930 ± 0.03	4.35 ± 0.06
GST-CD98-hBD3ox[b]	19.6 ± 0.09	13.05 ± 0.03	4.04 ± 0.06	0.682 ± 0.004	9.60 ± 0.09
CD98-6His-hBD3[b]	2.53 ± 0.05	1.79 ± 0.06	6.48 ± 0.02	1.865 ± 0.03	15.84 ± 0.06
CD98-6His-hBD3[c]	4.26 ± 0.06	2.25 ± 0.07	7.24 ± 0.05	2.163 ± 0.04	12.13 ± 0.07
CD98-6His-hBD3ox[b]	31.24 ± 0.05	40.79 ± 0.02	2.49 ± 0.09	0.456 ± 0.004	20.22 ± 0.09
GST-CD98cut-hBD3[b]	4.65 ± 0.07	1.26 ± 0.03	5.44 ± 0.06	0.907 ± 0.007	3.86 ± 0.07
GST-CD98cut-hBD3ox[b]	26.20 ± 0.02	8.88 ± 0.04	4.23 ± 0.08	0.604 ± 0.003	4.23 ± 0.08
hBD3-GST-CD98[c]	6.23 ± 0.08	1.28 ± 0.06	5.78 ± 0.07	1.500 ± 0.04	3.99 ± 0.08
hBD3-GST-CD98cut[c]	5.97 ± 0.09	0.627 ± 0.007	8.58 ± 0.08	0.969 ± 0.006	1.07 ± 0.09

[a]The first immobilized compound.
[b]CM4 sensor chip.
[c]CM5 sensor chip.

prognosis (Feng et al., 2006; Shames et al., 2010; Charania et al., 2013). It has been suggested that promotion of tumorigenesis is mediated by the interaction of CD98 with β_1-integrins (Cantor and Ginsberg, 2012; Furuya et al., 2012; Kaira et al., 2011). Since downregulation of CD98 promotes cell death via apoptosis (Bulus et al., 2012), the protein has been proposed as a therapeutic target (Santiago-Gómez et al., 2013).

The affinity of hBD3 toward CD98 is within micromolar range. The ectodomain of CD98 consists of two domains: an N-terminal globular domain adopts a triosephosphate isomerase (TIM) barrel fold (residues W218–K532) and a C-terminal domain presents a β-sandwich-like topology (residues D540–A630) (Figure 7B). We unambiguously mapped the hBD3-interacting region to CD98 residues V304–H414, i.e. to the region of the protein that interacts with the proteins of EPEC and *C. rodentium* (Shames et al., 2010; Charania et al., 2013). This region, which corresponds to almost half the β barrel, is built of four β strands belonging to the barrel and three amphipathic α helices surrounding the barrel. In such a type of fold, a ligand binding site often lies in a cavity at the top of the barrel, and the loops connecting the C terminus of the β strands to the adjacent α helices provide the key ligand binding residues. In the CD98 region that interacts with the highly charged hBD3, the loops contain a large number of negatively charged residues (see Figure 7C). We propose that this complementary charge interaction is the structural determinant for CD98-hBD3 recognition, as observed for the electrostatic interaction of hBD3 with the melanocortin and chemokine receptors (Nix et al., 2013; Esseghir et al., 2006).

The affinity of hBD3 toward CD98 depends little on the defensin oxidation state, as does the antimicrobial activity of the molecule (Scudiero et al., 2010, 2013). However, our kinetic data, obtained by SPR, revealed some differences, particularly in the association phase. This is due to the distinct 3D structure of the two hBD3 states (see Text S1). Although kinetic parameters are different, the resulting affinity of the two hBD3 forms toward CD98 is comparable (Table 1). The formation of the complex between hBD3 and CD98 does not rule out the occurrence of multipartner complexes.

To verify the physiological relevance of the proteomic and in vitro data, we first evaluated the colocalization of CD98 with hBD3, and found extensive colocalization on the basolateral domain of epithelial cells (Figure 4A). This result is consistent with studies reporting CD98 in the basolateral domain of epithelial cells (Mburu et al., 2011; Kaira et al., 2011). We also demonstrated, by FRET, direct binding of CD98 and hBD3 in cells fixed and coimmunostained with CD98 and biotin-hBD3 (Figure 4B). Furthermore, the specificity of CD98/BD3 binding is strongly supported by the results of the competition binding assay (Figure 5), which indicates that once hBD3 binds to the cell surface, this binding is specific and occurs with an affinity consistent with the KD obtained in SPR experiments. Having established the hBD3-CD98 interaction in vitro and in cells, we then asked if CD98 could play a functional role in the antibacterial activity of hBD3. Our SPR data suggest that hBD3 could act through competition with microbial ligands for the region of CD98 that enables bacterial invasion (Shames et al., 2010). In addition, we hypothesized that hBD3 might downregulate the expression of CD98, which would have a further inhibitory effect on bacterial invasion (Feng et al., 2006). This mechanism would be similar to that identified for the HIV coreceptor CXCR4 in human oral epithelial and immunocompetent cells, the internalization and downregulation of which are modulated by both hBD2 and hBD3 (Esseghir et al., 2006; Cai et al., 2005).

As shown in Figure S5, treatment of A549 cells with hBD3 dramatically reduced the expression of CD98 24 hr post treatment. Our analysis of hBD3 internalization showed that, after this interaction, hBD3 is internalized by means of recycling endosomes (Figures 2A, 2B, and 6) and accumulates with transferrin (Figure 2B), suggesting that hBD3 avoids lysosome degradation and is sorted back to the cell surface. This would enable the peptide to downregulate CD98 to reduce invasion and to exert direct antibacterial activity at the surface epithelium.

In conclusion, our results suggest an additional mechanism whereby hBD3 exerts antibacterial activity, namely, a mechanism involving its accumulation on mucosal surfaces. Moreover, since CD98 is overexpressed in several tumors and is associated with a poor prognosis (Cantor and Ginsberg, 2012; Furuya et al., 2012), one could speculate that hBD3 plays a role also in the innate immune surveillance of malignancy. For both activities, the moderate (μM) affinity of the hBD3-CD98 interaction would ensure that binding and the ensuing downregulation are maximized in CD98-overexpressing cells, thereby leaving the cells

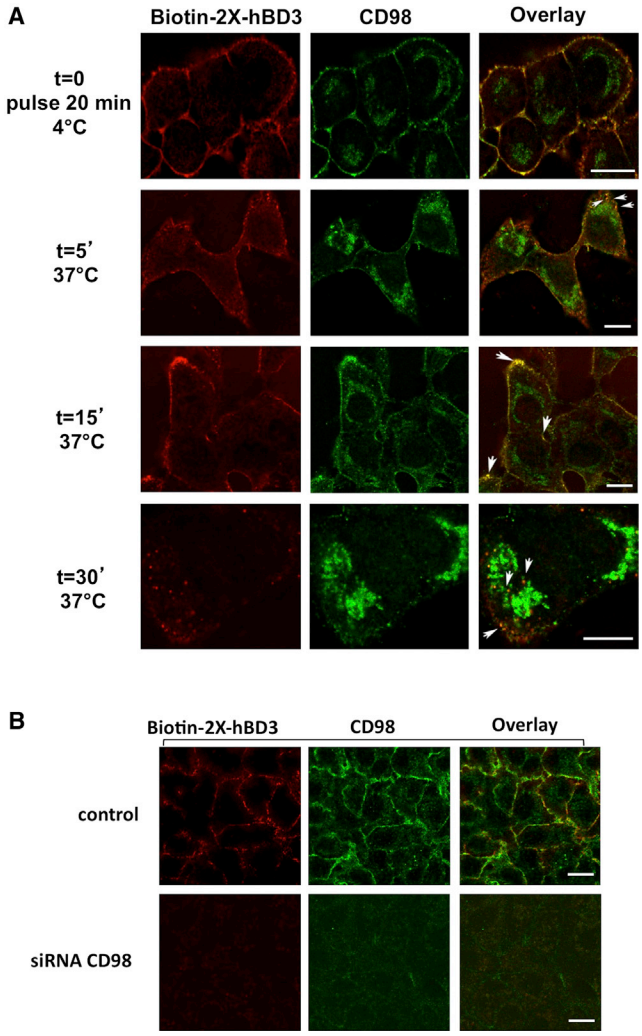

Figure 6. Biotin-2X-hBD3 and CD98 Internalization

(A) A549 cells were grown on filters for 72 hr, incubated with the peptide (10 μM) for 20 min at 4°C (pulse), then washed and immunostained with CD98. Biotin-2X-hBD3 colocalized with CD98 at different chase times: 0 min, 5 min, 15 min, 30 min. Scale bars, 10 μm. Images represent single 1-μm-thick optical slices. Biotin-2X-hBD3 is red and CD98 green; colocalizing regions appear orange-yellow in the overlay image (see arrows). Three independent experiments were performed, and images were acquired from at least 100 cells per experiment.

(B) Biotin-2X-hBD3 does not bind the plasma membrane and is not internalized into A549 cells when CD98 is silenced. CD98 was silenced using a specific siRNA for 72 hr in A549 cells. Then, cells were incubated with the peptide (10 μM) for 20 min at 4°C (pulse), then washed and immunostained with CD98. A549 cells were incubated with the peptide (10 μM) for 20 min at 4°C (pulse), washed, incubated at 37°C and labeled with CD98. Biotin-2X-hBD3 is red, CD98 is green. Three independent experiments were performed, and images were acquired from at least 100 cells per experiment. See also Figures S4 and S5.

with normal CD98 expression unperturbed. Moreover, the identification of the specific region of interaction between hBD3 and CD98 may be exploited to design higher-affinity hBD3 variants for possible therapeutic applications. The novel findings of this study pave the way for further development toward a therapeutic approach.

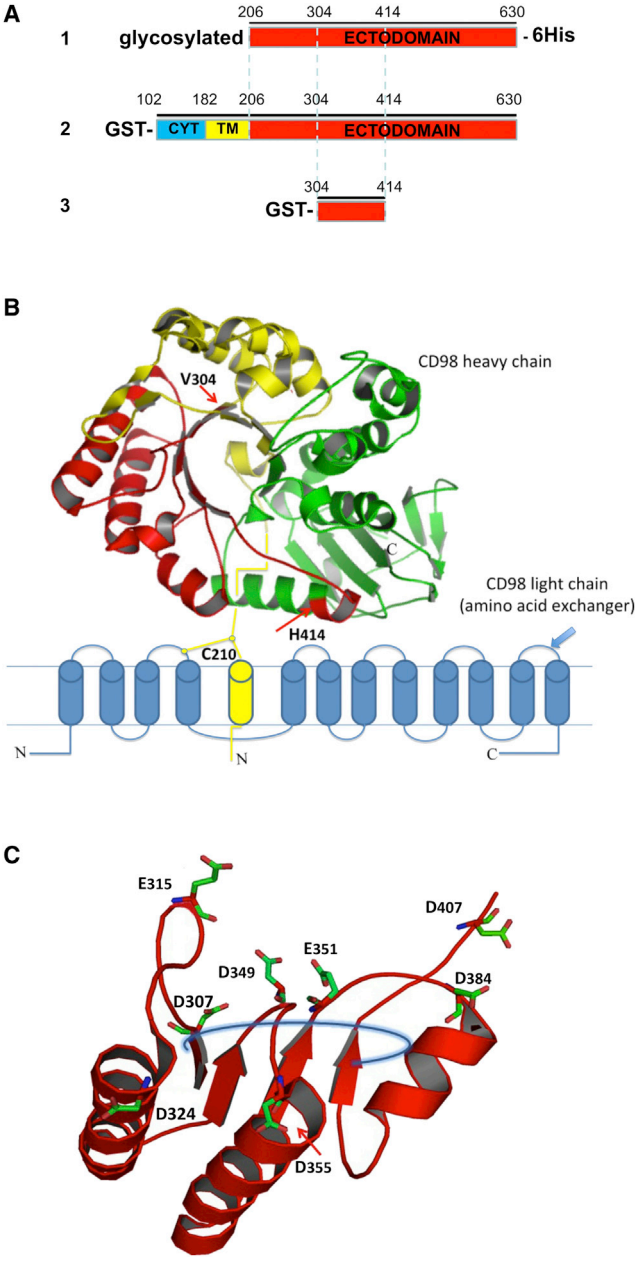

Figure 7. Characterization of CD98-hBD3 Interaction

(A) The selected CD98 sequencing regions studied as interactors of hBD3 peptide by SPR.

(B) Schematic representation of the whole CD98 heterodimer. (Top) Ribbon representation of the CD98 heavy domain from the Protein Data Bank file 2DH2. In this view, the TIM barrel fold is clearly visible from the top of the β barrel with surrounding α helices. The region (V304–H414) interacting with hBD3 is drawn in red. The preceding and following protein regions are colored in yellow and green, respectively. (Bottom) Cartoon of the transmembrane light chain helices (blue) linked by a disulfide bond involving C210 of the heavy domain.

(C) A close-up view of the interacting region consisting of four β strands (belonging to the barrel) and three α helices. Numerous negative residues (labeled) lie on the loops connecting the strands to the helices, at the top of the barrel. The blue semicircle traces the barrel closure. See also Figure S6.

SIGNIFICANCE

hBD3 exerts antimicrobial activity at epithelial surfaces through a variety of mechanisms. With its highly positively charged amphipathic structure stabilized by a triple-disulfide bond, it is able to severely damage the bacterial membranes, while being readily internalized into host cells. Here, we show that internalization of hBD3 in lung A549 cells is assisted by CD98, a multifunctional transmembrane protein. The binding site of hBD3 is located in a CD98 negatively charged pocket, which coincides with the region bound by the intestinal bacteria EPEC and *C. rodentium* during invasion of colonic tissue. Notably, hBD3 binding also downregulates CD98 expression. Our study reveals a novel antimicrobial mechanism of hBD3, i.e. competitive binding for a bacterial invasion receptor driven by electrostatic complementarity. This mechanism may apply to other defensin-receptor partners yet to be discovered.

EXPERIMENTAL PROCEDURES

Biotinylated Peptide Synthesis

The reduced form of hBD3 was synthesized using standard 9-fluorenylmethoxycarbonyl (Fmoc) solid-phase methods, as previously reported (Scudiero et al., 2010, 2013), and purified by preparative reverse-phase-high pressure liquid chromatography (RP-HPLC) on a C18 column (2 x 250 mm, 5 μm, Phenomenex), using as solvent system H_2O/0.1% TFA (A) and CH_3CN/0.1% TFA (B), and a linear gradient 5%–50% B over 17 min, flow rate 20 ml/min. Analytical RP-HPLC used a Phenomenex C18 column (4.6 x 250 mm, 5 μm). The identity of the purified peptides was confirmed by electron spray ionization liquid chromatography-mass spectrometry (ESI LC-MS) using a Thermo Electron MSQ Surveyor. Biotin labeling of the reduced hBD3 was performed on the resin-bound peptide. Briefly, 70 mg of resin-bound peptide (25 μmol) was treated with piperidine in dimethylformamide to remove the Fmoc group and then reacted for 24 hr with 2X-AH-biotin-*N*-hydroxysuccinimide ester (Biotin-2X, Sigma-Aldrich) in the presence of 4-dimethylaminopyridine (Sigma-Aldrich). Cleavage conditions were the same as for the unlabeled peptide. Compound identity was confirmed by LC/MS. The oxidized form of HBD3 was purchased from Peptides International.

Antibacterial Activity Assay

For the colony-forming unit (CFU) assays of antibacterial activity against *E. coli* (ATCC 25922), the strain was grown under aerobic conditions in tryptic soy broth (Difco Laboratories) at 37°C and incubated with the peptide for 2 hr at 37°C. Two peptide concentrations, 2.5 μM and 12.5 μM, were used. For the salt dependence assay, 0.0, 50, 100, and 200 mM NaCl were included in the incubation buffer, as reported elsewhere (Scudiero et al., 2013). Each assay was performed in triplicate. The minimum inhibitory concentration of the three peptides was determined with the modified version of the broth microdilution assay of the Clinical and Laboratory Standards Institute, using a final inoculum concentration of 10^5 cfu/ml. The peptide concentrations were 100, 50, 25, 12.5, 6.25, 3.12, and 1.56 μM.

Cell Culture

A549 cells were obtained from the Bank of Human and Animal Continuous Cell Lines (CEINGE-Biotecnologie Avanzate). A549 were grown in 90% DMEM (Sigma-Aldrich) supplemented with 10% fetal bovine serum (FBS) (Lonza) and 1% *L*-glutamine (Sigma-Aldrich). The cells were grown as a monolayer in a flask at 37°C in 5% CO_2.

A549 Cell Transfection by CD98 siRNA

The CD98-specific and scrambled control siRNAs were obtained from Novus Biologicals. Transfection of A549 cells was performed using LipofectAMINE2000 (Invitrogen) according to the manufacturer's instructions.

Formaldehyde Crosslinking

A549 cells (2 x 10^6) were plated on 100 mm dishes and cultured in DMEM containing 10% FBS for 48 hr. Cells were washed three times with PBS and then incubated for 20 min at 4°C with Biotin-hBD3 (10 μM in H_2O) or with 10 μM Biotin-2X in H_2O as control. Biotin-hBD3 was crosslinked to putative interacting proteins using formaldehyde, which efficiently produces reversible protein-protein crosslinks in vivo (Sutherland et al., 2008; Klockenbusch and Kast, 2010). Cells were treated with a 1.0% w/v solution of paraformaldehyde in PBS at room temperature. Formaldehyde crosslinking was allowed to proceed for 10 min at room temperature, then the reaction was quenched by addition of 1.25 M glycine to a final concentration of 125 mM, for 5 min at room temperature. Cells were harvested, washed twice with PBS, and then treated with the Subcellular Protein Fractionation Kit (Pierce Biotechnology) to isolate plasma, mitochondria, and ER/Golgi membrane components, excluding nuclear membranes. Cell lysates were centrifuged for 15 min at 14,000 rpm to precipitate cell debris. Supernatants were collected and protein levels quantified using a BCA protein assay kit (Pierce Biotechnology).

Affinity Chromatography

To isolate peptide-protein complexes, protein extracts were incubated with Mag*Strep* type 2HC magnetic beads (IBA) using 40 μl of extract/mg of beads, containing IP buffer (Tris-HCl 50 mM [pH 7.5], NaCl 150 mM, NaF 1 mM, PMSF 1 mM, Nonidet P-40 1%, 1 mM EDTA, 1 mM sodium orthovanadate) and Protease inhibitor cocktail (Complete mini EDTA-free, Roche Applied Science), for 30 min at 4°C on a rocker platform. Supernatants were then separated from the beads using a magnetic separator. After extensive washing of the pellet beads with IP buffer, the resulting peptide-protein complexes were decrosslinked and eluted from the beads with 2× electrophoresis sample buffer at 90°C for 10 min. The protein mixture was then resolved by electrophoresis on 10% SDS-PAGE and stained with Coomassie brilliant blue (Pierce Biotechnology). Each lane of the gel was cut into slices and processed for LC-MS/MS analysis.

Western Blotting

For Western blot analysis, proteins were resolved by 10% SDS-PAGE and then transferred onto nitrocellulose membranes (GE Healthcare) by Mini Trans-Blot electrophoretic transfer (Bio-Rad). Membranes were blocked using 5% nonfat milk in PBS (pH 7.5) for 2 hr and then immunoblotted with antibodies against histone H3 (1:1000), EGFR (1:1000), GAPDH (1:2000), CD98 (1: 250) (Santa Cruz Biotechnology), anti-H3 (Abcam), and Hrp-conjugated streptavidin (Cell Signaling Technology). The Western blot images obtained were scanned by PDquest 7.1 software (Bio-Rad). The protein band images on X-ray films were acquired with the Chemidoc XRS system (Bio-Rad). GAPDH was used as loading control, since it is equally expressed in all the cell lines considered. We used the Quantity One 4.5 tool (Bio-Rad) for densitometric measurements.

LC-MS/MS and Data Analysis

Gel slices were placed in Eppendorf tubes and washed with 50 mM ammonium bicarbonate for 10 min, and destained twice with 50 mM ammonium bicarbonate followed by acetonitrile for 15 min. The gel slices were dehydrated by incubation with acetonitrile for 15 min and vacuum dried in a SpeedVac. The dried gel slices were treated with proteomics grade trypsin (Sigma-Aldrich) at 37°C overnight. The samples were briefly spun and supernatants were transferred to clean dry Eppendorf tubes. Peptides were further extracted from the gel once with 0.1% trifluoroacetic acid in 50% acetonitrile for 10 min followed by acetonitrile for 20 min at 37°C. Pooled supernatants were dried in a SpeedVac. Before LC-MS/MS analysis, the samples were reconstituted with 10 μl of 0.2% formic acid. LC-MS/MS analysis was performed on an LC/MSD Trap XCT Ultra system equipped with a 1100 HPLC-Chip Cube interface (Agilent Technologies). The peptide sample was concentrated and washed on a 40-nl enrichment column (Agilent Technologies chip), using as eluent 0.1% formic acid at 4 μl/min, then fractionated on a C18 reverse-phase capillary column (75 μm x 43 mm) using a flow rate of 200 nl/min and a linear gradient of 5%–60% acetonitrile in 2% formic acid. Subsequently, we analyzed the peptides using data-dependent acquisition of one MS scan (mass range from 400 to 2000 *m/z*) followed by MS/MS scans of the three most abundant ions. To obtain a more detailed survey of the peptides, we carried out dynamic exclusion using a procedure of automatic recognition and temporary exclusion

(2 min) of ions from which definitive mass spectral data had previously been acquired.

Data were analyzed with MASCOT software (version 2.4) Peptide Mass Fingerprinting search program (http://www.matrixscience.com), selecting the NCBInr aug2010 database (11592891 sequences, http://www.ncbi.nlm.nih.gov), and the following six parameters: specificity of the proteolytic enzyme used for hydrolysis (trypsin) up to 1 missed cleavage; Cys such as *S*-carbamidomethyl Cys; unmodified N- and C-terminal ends; unmodified and oxidized methionines; putative Gln-induced pyroGlu formation; a precursor peptide maximum mass tolerance of 400 ppm and a maximum fragment mass tolerance of 0.6 Da. Using the probability-based Mowse score, the ion score is −10 x log(*P*), *P* being the probability that an eventual match is a random occurrence. All MS/MS spectra with a MASCOT score >41 ($p \leq 0.05$) had a good signal to noise ratio, so the interpretation of the data was unambiguous. MS/MS spectra of peptides that had a MASCOT score <41 were inspected manually and included in the statistics only in the presence of at least four continuous *y* or *b* ions. We also used the BLAST program (http://ncbi.nlm.nih.gov/blast) and the NCBI database to search for the peptide sequence. Peptides with an ambiguous identification were removed from the list. Specifically, the candidate protein was deleted from the list when it matched other proteins. Protein species identified by a single peptide were examined further. We manually reconstructed the peptide sequence stretch, and analyzed it and the precursor ion mass with the MASCOT software set in the sequence query mode. Proteins found also in the control samples were considered nonspecific and excluded from the list of identified proteins.

Confocal Microscopy

A549 cells were seeded at 25% confluence in WillCo glass bottom dishes (WillCo Wells) or Transwell clear Constar filters (3460). For plasma membrane localization, cells were incubated with 10 μM of Biotin-2X-hBD3 for 20 min at 4°C (pulse); hBD3-containing medium was then replaced with fresh growth medium and cells were incubated with streptavidin-Cy3, washed and stained with a rabbit (BD-Bioscience) primary antibody against a marker of the basolateral cell membrane (E-cadherin) followed by an Alexafluor 488-conjugated secondary antibody. The samples were fixed with 3% paraformaldehyde (Sigma-Aldrich) and analyzed by confocal laser scanning microscopy. To ensure that neither biotin nor streptavidin interferes with fluorescent signals, we used cells treated with biotin and stained with streptavidin-Cy3 as controls; no fluorescence signal was detected (data not shown).

Internalization Assay by Fluorescence Microscopy

A549 cells were grown on glass bottom dishes for 24 hr, washed with PBS, and processed for the endocytic assay. Briefly, cells were incubated with both 10 μM of Biotin-2X-hBD3 and transferrin-Alexa 488 conjugated for 20 min at 4°C (pulse). Then the cells were warmed at 37°C for the indicated times (chase) to allow hBD3 and transferrin internalization, and were fixed with paraformaldehyde 3%, permeabilized with TX-100 0.1% in PBS/BSA 1% for 10 min and incubated with streptavidin-Cy3 for 20 min to label hBD3.

FRET

A549 cells seeded in WillCo glass bottom dishes (35/22 mm) were grown in DMEM supplemented with 10% fetal calf serum and 1% *L*-glutamine. FRET experiments were performed 24 hr post plating. FRET was measured with the acceptor photobleaching technique (Kenworthy and Edidin, 1999) where, upon irreversible photobleaching, the donor fluorescence increase was recorded. Cells were incubated with 10 μM Biotin-2X-hBD3 for 20 min at 4°C followed by Cy5-conjugated streptavidin to specifically label Biotin-2X -hBD3. After fixation, cells were immunostained with specific goat primary anti-CD98 antibody (Santa Cruz Biotechnology) and revealed by secondary anti-goat Cy3-conjugated antibody. Acceptor photobleaching experiments were performed with the Leica TCS SMD SP5 confocal microscope with an oil immersion 63x (numerical aperture 1.4) objective lens. Excitation at 561 and 633 nm was used for Cy3 and Cy5, respectively. For Cy5 bleaching, the 633 nm He-Ne laser light with 100% output power was used and pinhole diameters were set to 1.0 μm optical slices. FRET measurements were obtained with the LAS AF software (Leica) after photobleaching of a selected squared region of interest. We calculated FRET efficiency using the following equation: *E* = (fluorescence intensity of Cy3 after bleaching − fluorescence intensity of Cy3 before bleaching)/fluorescence intensity of Cy3 after bleaching.

As control: (1) we measured FRET on cells immunostained with primary anti-CD98 followed by Cy3-conjugated secondary antibody alone to ensure that photobleaching per se does not affect the fluorescence of the donor and that photoconversion does not occur during the photobleaching analysis; and (2) as indicated in Figure 4, we stained cells with primary anti-CD98 and secondary-Cy3 conjugated antibody followed by labeling with streptavidin-Cy5 without Biotin-2X-hBD3 incubation. We calculated the background raised by the photobleaching per se by bleaching Cy5 in cells negative for this fluorophore. The background value was subtracted from all samples. All the experiments were done in triplicate and data are means ± SD of three independent experiments.

Competition Binding Assay

To select the peptide concentration at which to perform the competition assay, different concentrations of labeled Biotin-2X-hBD3 were incubated with the cells to obtain a titration curve. Confocal images of cells incubated with different concentrations of Biotin-2X-hBD3 were evaluated for fluorescence intensity with the LAS AF software considering the signal deriving from the 10 μM hBD3 incubation as 100%. Data were normalized by analyzing the same area for all samples. A concentration of 3 μM was chosen by extrapolation of the linear trend for the competition assay. A549 cells were grown in normal growth medium on WillCo glass bottom dishes. On the day of the analysis, the medium was removed and cells were washed twice with cold PBS and the required concentration of unlabeled (hBD3) or labeled (Biotin-2X-hBD3) compound was added. Briefly, the cells were first incubated with labeled Biotin-2X-hBD3 for 20 min at 4°C, washed twice and increasing amounts of unlabeled hBD3 were added for a further 20 min on ice. Conversely, the cells were first incubated with unlabeled hBD3 for 20 min at 4°C, washed and then stained with labeled Biotin-2X-hBD3. hBD3 was revealed by streptavidin Cy3-conjugated. In both cases, CD98 was revealed with the same procedure described elsewhere (Stoddart et al., 2012).

SPR

SPR experiments were performed using a Biacore T200 system (GE Healthcare) at 25°C. Binding assays were carried out between various CD98 sequences and both reduced and oxidized hBD3. Hereafter residue numbering is referred to CD98 isoform-1.

First, the protein sequences GST-CD98 (102–630) (Novus Biologicals), CD98-6His (206–630) (Novoprotein), and the truncated GST-CD98 (304–414) (Novus Biologicals) were immobilized on a CM4 and/or a CM5 sensor chip (research grade) by the standard amine coupling procedure, using HBS-EP buffer (HEPES 10 mM, NaCl 150 mM, EDTA 3 mM, Surfactant P20 0.005% [pH 7.4]), as running buffer. The CD98 forms were immobilized through activation of the sensor chip with 60 μl of *N*-hydroxysuccinimide and *N*-ethyl-*N*-(dimethylaminopropyl)-carbodiimide at 10 μl/min, followed by a 30 μl injection of CD98 forms diluted in 10 mM sodium acetate buffer (pH 4.0). Unreacted activated groups were blocked by a 60 μl injection of 1 M ethanolamine at 10 μl/min. The final CD98 immobilized levels were typically between ~1,500 and 5,000 RU, corresponding to a protein concentration of 15 ÷ 50 mg/ml on the surface layer. Subsequently, both reduced and oxidized hBD3 were injected as analyte at various concentrations (from 100 nM to 100 μM), and using the same HBS-EP buffer as running buffer. All binding assays were performed under various conditions: (1) a contact time of 60 s and 120 s and a dissociation time of 600 s and 1000 s to evaluate the best kinetic model; (2) a flow rate of 30 and 60 μl/min to evaluate the contribution of mass transport.

Second, hBD3 was immobilized on a CM5 sensor chip (research grade) by the standard amine coupling procedure, using HBS-EP buffer as running buffer, under the same conditions as described above. After the sensor chip activation as before, 30 μl of hBD3 diluted in 10 mM sodium acetate buffer (pH 5.5) was injected and finally unreacted activated groups were blocked as described above. Then, the two GST-fused CD98 protein sequences were injected as analytes at various concentrations (from 20 nM to 20 μM), and using HBS-EP buffer as running buffer. As control, GST was immobilized on a CM5 sensor chip and hBD3 was allowed to flow, following the procedure described above.

The SPR sensorgrams for each CD98-hBD3 interaction were analyzed by curve fitting using the Biacore T200 Evaluation software. Dose-response curves were plotted using the SPR sensorgrams and the corresponding fit. Various reaction models were used to perform a complete kinetic analysis of the sensorgrams, and the best fitting was considered in such a way that the χ^2 value, representing the statistical closeness of curve fitting, became the lowest. The two-state reaction model (including a conformational change) was chosen, which is described as

$$A + B \rightleftarrows AB \rightleftarrows AB^*$$

where A is the immobilized CD98 form, B is hBD3, AB represents the protein-hBD3 complex and AB* represents the stable complex after the conformational change. The binding KD was calculated from the equation

$$K_D = \frac{k_{off1}}{k_{on1}} \times \frac{k_{off2}}{(k_{off2} + k_{on2})}$$

SUPPLEMENTAL INFORMATION

Supplemental Information includes six figures and Text S1 and can be found with this article online at http://dx.doi.org/10.1016/j.chembiol.2014.11.020.

AUTHOR CONTRIBUTIONS

F.S. and A.P. conceived the research and directed and discussed the comprehensive assembly of data acquisition; I.C. and E.N. did most of the experimental work by conceiving it and analyzing and discussing the data obtained by studying defensin and cell receptor interaction; D.S. did the major experimental work by conceiving it and discussed the data concerning results obtained after confocal microscopy and FRET experiments; E.N., I.C., O.S., A.D., and D.S. performed or coordinated the laboratory experimental work and data acquisition; A.Z., V.G., and I.C. conceived the experimental approach by SPR and analyzed and discussed the results obtained in the frame of the general data acquisition; F.S., A.P., A.D., and A.Z., with E.N. and I.C., wrote the manuscript, but all authors supervised and helped with the final version.

ACKNOWLEDGMENTS

We thank Jean Ann Gilder (Scientific Communication, Naples, Italy) for revising and editing the text; and Vittorio Lucignano, CEINGE-Biotecnologie Avanzate, for technical assistance. This work was supported by Grant PON01_02589 (MICROMAP) - 2012 and Grant PON02_00677 (BIOGENE) potenziamento lab.8 – 2012 from the Italian Ministry of University and Research (both to F.S.); Grant POR Campania FSE 2007/2013 (CAMPUS-Bioframe) from the Regione Campania, Italy (to F.S.)

Received: September 15, 2014
Revised: November 15, 2014
Accepted: November 20, 2014
Published: January 29, 2015

REFERENCES

Beaumont, K.A., Smit, D.J., Liu, Y.Y., Chai, E., Patel, M.P., Millhauser, G.L., Smith, J.J., Alewood, P.F., and Sturm, R.A. (2012). Melanocortin-1 receptor-mediated signalling pathways activated by NDP-MSH and hBD3 ligands. Pigment Cell Melanoma Res. *25*, 370–374.

Bulus, N., Feral, C., Pozzi, A., and Zent, R. (2012). CD98 increases renal epithelial cell proliferation by activating MAPKs. PLoS One *7*, e40026.

Cai, S., Bulus, N., Fonseca-Siesser, P.M., Chen, D., Hanks, S.K., Pozzi, A., and Zent, R. (2005). CD98 modulates integrin β1 function in polarized epithelial cells. J. Cell Sci. *118*, 889–899.

Cantor, J.M., and Ginsberg, M.H. (2012). CD98 at the crossroads of adaptive immunity and cancer. J. Cell Sci. *125*, 1373–1382.

Charania, M.A., Laroui, H., Liu, H., Viennois, E., Ayyadurai, S., Xiao, B., Ingersoll, S.A., Kalman, D., and Merlin, D. (2013). Intestinal epithelial CD98 directly modulates the innate host response to enteric bacterial pathogens. Infect Immun. *81*, 923–934.

Cronican, J.J., Beier, K.T., Davis, T.N., Tseng, J.C., Li, W., Thompson, D.B., Shih, A.F., May, E.M., Cepko, C.L., Kung, A.L., et al. (2011). A class of human proteins that deliver functional proteins into mammalian cells in vitro and in vivo. Chem. Biol. *18*, 833–838.

Dhople, V., Krukemeyer, A., and Ramamoorthy, A. (2006). The human beta-defensin-3, an antibacterial peptide with multiple biological functions. Biochim. Biophys. Acta *1758*, 1499–1512.

Esseghir, S., Reis-Filho, J.S., Kennedy, A., James, M., O'Hare, M.J., Jeffery, R., Poulsom, R., and Isacke, C.M. (2006). Identification of transmembrane proteins as potential prognostic markers and therapeutic targets in breast cancer by a screen for signal sequence encoding transcripts. J. Pathol. *210*, 420–430.

Feng, Z., Dubyak, G.R., Lederman, M.M., and Weinberg, A. (2006). Cutting edge: human beta defensin 3–a novel antagonist of the HIV-1 coreceptor CXCR4. J. Immunol. *177*, 782–786.

Furuya, M., Horiguchi, J., Nakajima, H., Kanai, Y., and Oyama, T. (2012). Correlation of L-type amino acid transporter 1 and CD98 expression with triple negative breast cancer prognosis. Cancer Sci. *103*, 382–389.

Ganz, T. (2003). Defensins: antimicrobial peptides of innate immunity. Nat. Rev. Immunol. *3*, 710–720.

Harder, J., Bartels, J., Christophers, E., and Schroder, J.M. (2001). Isolation and characterization of human beta -defensin-3, a novel human inducible peptide antibiotic. J. Biol. Chem. *276*, 5707–5713.

Jarczak, J., Kosciuczuk, E.M., Lisowski, P., Strzalkowska, N., Jozwik, A., Horbańczuk, J., Krzyżewski, J., Zwierzchowski, L., and Bagnicka, E. (2013). Defensins: natural component of human innate immunity. Hum. Immunol. *74*, 1069–1079.

Jason-Moller, L., Murphy, M., and Bruno, J. (2006). Overview of Biacore systems and their applications. Curr. Protoc. Protein. Sci. *19*, 13.

Kaira, K., Ohde, Y., Endo, M., Nakagawa, K., and Okumura, T. (2011). Expression of 4F2hc (CD98) in pulmonary neuroendocrine tumors. Oncol. Rep. *26*, 931–937.

Kenworthy, A.K., and Edidin, M. (1999). Imaging fluorescence resonance energy transfer as probe of membrane organization and molecular associations of GPI-anchored proteins. Methods Mol. Biol. *116*, 37–49.

Klockenbusch, C., and Kast, J. (2010). Optimization of formaldehyde cross-linking for protein interaction analysis of non-tagged integrin beta1. J. Biomed. Biotechnol. *2010*, 1–13.

Miranda, K.C., Joseph, S.R., Yap, A.S., Teasdale, R.D., and Stow, J.L. (2003). Contextual binding of p120ctn to E-cadherin at the basolateral plasma membrane in polarized epithelia. J. Biol. Chem. *278*, 43480–43488.

Mburu, Y.K., Abe, K., Ferris, L.K., Sarkar, S.N., and Ferris, R.L. (2011). Human β-defensin 3 promotes NF-κB-mediated CCR7 expression and anti-apoptotic signals in squamous cell carcinoma of the head and neck. Carcinogenesis *32*, 168–174.

Nguyen, H.T., Dalmasso, G., Torkvist, L., Halfvarson, J., Yan, Y., Laroui, H., Shmerling, D., Tallone, T., D'Amato, M., Sitaraman, S.V., and Merlin, D. (2011). CD98 expression modulates intestinal homeostasis, inflammation, and colitis-associated cancer in mice. J. Clin. Invest. *121*, 1733–1747.

Nguyen, H.T., and Merlin, D. (2012). Homeostatic and innate immune responses: role of the transmembrane glycoprotein CD98. Cell Mol. Life Sci. *69*, 3015–3026.

Nix, M.A., Kaelin, C.B., Ta, T., Weis, A., Morton, G.J., Barsh, G.S., and Millhauser, G.L. (2013). Molecular and functional analysis of human β-defensin 3 action at melanocortin receptors. Chem. Biol. *20*, 784–795.

Quiñones-Mateu, M.E., Lederman, M.M., Feng, Z., Chakraborty, B., Weber, J., Rangel, H.R., Marotta, M.L., Mirza, M., Jiang, B., Kiser, P., et al. (2003). Human epithelial beta-defensins 2 and 3 inhibit HIV-1 replication. AIDS *17*, F39–F48.

Röhrl, J., Yang, D., Oppenheim, J.J., and Hehlgans, T. (2010). Human beta-defensin 2 and 3 and their mouse orthologs induce chemotaxis through interaction with CCR2. J. Immunol. *184*, 6688–6694.

Santiago-Gómez, A., Barrasa, J.I., Olmo, N., Lecona, E., Burghardt, H., Palacín, M., Lizarbe, M.A., and Turnay, J. (2013). 4F2hc-silencing impairs

tumorigenicity of HeLa cells via modulation of galectin-3 and β-catenin signaling, and MMP-2 expression. Biochim. Biophys. Acta *1833*, 2045–2056.

Sass, V., Schneider, T., Wilmes, M., Körner, C., Tossi, A., Novikova, N., Shamova, O., and Sahl, H.G. (2010). Human beta-defensin 3 inhibits cell wall biosynthesis in Staphylococci. Infect. Immun. *78*, 2793–2800.

Scudiero, O., Galdiero, S., Cantisani, M., Di Noto, R., Vitiello, M., Galdiero, M., Naclerio, G., Cassiman, J.J., Pedone, C., Castaldo, G., and Salvatore, F. (2010). Novel synthetic, salt-resistant analogs of human beta-defensins 1 and 3 endowed with enhanced antimicrobial activity. Antimicrob. Agents Chemother. *54*, 2312–2322.

Scudiero, O., Galdiero, S., Nigro, E., Del Vecchio, L., Di Noto, R., Cantisani, M., Colavita, I., Galdiero, M., Cassiman, J.J., Daniele, A., et al. (2013). Chimeric beta-defensin analogs, including the novel 3NI analog, display salt-resistant antimicrobial activity and lack toxicity in human epithelial cell lines. Antimicrob. Agents Chemother. *57*, 1701–1708.

Semple, F., and Dorin, J.R. (2012). β-Defensins: multifunctional modulators of infection, inflammation and more? J. Innate Immun. *4*, 337–348.

Shames, S.R., Deng, W., Guttman, J.A., de Hoog, C.L., Li, Y., Hardwidge, P.R., Sham, H.P., Vallance, B.A., Foster, L.J., and Finlay, B.B. (2010). The pathogenic *E. coli* type III effector EspZ interacts with host CD98 and facilitates host cell prosurvival signalling. Cell Microbiol. *12*, 1322–1339.

Smith, J.J., Travis, S.M., Greenberg, E.P., and Welsh, M.J. (1996). Cystic fibrosis airway epithelia fail to kill bacteria because of abnormal airway surface fluid. Cell *85*, 229–236.

Soruri, A., Grigat, J., Forssmann, U., and Riggert, J.Z. (2007). beta-Defensins chemoattract macrophages and mast cells but not lymphocytes and dendritic cells: CCR6 is not involved. Eur. J. Immunol. *37*, 2474–2486.

Stoddart, L.A., Vernall, A.J., Denman, J.L., Briddon, S.J., Kellam, B., and Hill, S.J. (2012). Fragment screening at adenosine-A(3) receptors in living cells using a fluorescence-based binding assay. Chem. Biol. *19*, 1105–1115.

Sudheendra, U.S., Dhople, V., Datta, A., Kar, R.K., Shelburne, C.E., Bhunia, A., and Ramamoorthy, A. (2014). Membrane disruptive antimicrobial activities of human β-defensin-3 analogs. Eur. J. Med. Chem. http://dx.doi.org/10.1016/j.ejmech.2014.08.021.

Sutherland, B.W., Toews, J., and Kast, J. (2008). Utility of formaldehyde cross-linking and mass spectrometry in the study of protein-protein interactions. J. Mass Spectrom. *43*, 699–715.

Thompson, D.B., Villaseñor, R.D., Brent, M., Zerial, M., and Liu, D.R. (2012). Cellular uptake mechanisms and endosomal trafficking of supercharged proteins. Chem. Biol. *19*, 831–843.

Yamaguchi, Y., and Ouchi, Y. (2012). Antimicrobial peptide defensin: identification of novel isoforms and the characterization of their physiological roles and their significance in the pathogenesis of diseases. Proc. Jpn. Acad. Ser. B Phys. Biol. Sci. *88*, 152–166.

Zorko, M., and Langel, U. (2005). Cell-penetrating peptides: mechanism and kinetics of cargo delivery. Adv. Drug Deliv. Rev. *57*, 529–545.

